

# The global communication pathways of the human brain transcend the cortical - subcortical - cerebellar division

Julian Schulte,<sup>1,2</sup> Mario Senden,<sup>3,4</sup> Gustavo Deco,<sup>1,2,5</sup> Xenia Kobeleva,<sup>6,7</sup> and Gorka Zamora-López<sup>1,2, a)</sup>

<sup>1)</sup> Center for Brain and Cognition, Pompeu Fabra University, Barcelona, Spain.

<sup>2)</sup> Department of Information and Communication Technologies, Pompeu Fabra University, Barcelona, Spain.

<sup>3)</sup> Department of Cognitive Neuroscience, University of Maastricht, Maastricht, The Netherlands.

<sup>4)</sup> Maastricht Brain Imaging Centre, Faculty of Psychology and Neuroscience, Maastricht University, Maastricht, The Netherlands.

<sup>5)</sup> Institució Catalana de la Recerca i Estudis Avançats (ICREA), Barcelona, Spain.

<sup>6)</sup> Computational Neurology Group, Department of Neurostimulation, Ruhr University Bochum, Bochum, Germany.

<sup>7)</sup> German Center for Neurodegenerative Diseases (DZNE) Bonn, Bonn, Germany.

Neural communication across the cortex, subcortex, and cerebellum is orchestrated by the structural connectome, forming the indispensable anatomical framework for capabilities spanning from elementary motor actions to higher cognitive functions. Yet, despite this importance, the core organizational rules that govern this connectivity remain insufficiently understood. Here we show, for the first time, how the integrated cortical, subcortical, and cerebellar brain areas shape the structural architecture of the whole brain. We find dense structural clusters, which differ in composition and arrangement, vertically transverse the canonical cortical, subcortical, and cerebellar boundaries. These clusters are centralized by a global rich club of predominantly subcortical, alongside cortical hub regions. Congruently, we find that subcortical hubs are not only the most widely connected brain areas but are also leading overall structural integration. Nearly all larger subcortical structures encompass these hub regions, but they also exhibit brain regions with fewer but more specialized connections, pointing toward functional heterogeneity in these structures themselves. Our findings move beyond traditional cortico-centric analysis, offering an initial and global perspective for understanding overall structural connectivity.

## INTRODUCTION

Complex cognition emerges from the coordinated activity of distributed brain regions. Yet, a historically dominant corticocentric perspective largely confined higher functions to the neocortex, and assigned supportive roles to the subcortical and cerebellar structures<sup>1,2</sup>. Converging evidence now critically challenges this sentiment, demonstrating for example, crucial contributions of the basal ganglia to cognition<sup>3</sup>, of the hippocampus to decision-making and reward<sup>4</sup>, and of the cerebellum to cognitive operations<sup>5,6</sup>. To embrace this emerging holistic view of brain function requires a shift towards understanding brain-wide integration, and thus, to consider its communication pathways at the system's level.

Studies of the white-matter connectivity at the large-scale in the mammalian brain (often referred as the structural connectivity or connectome) have revealed that this forms a hierarchically modular network, centralized by a set of hub regions (termed as the ‘rich-club’)<sup>7–9</sup>. The functional relevance of these hubs has been empirically corroborated for multisensory and cognitive integration<sup>10–12</sup>, and their dysfunction associated with multiple conditions<sup>13</sup>. So far, structural studies have mostly fo-

cused on cortico-cortical connections, ignoring the cerebellum. When included, subcortical structures are often treated as a single node, introducing an unbalanced combination of resolutions. For example, the thalamus is known to broadly connect with the cortex but these projections originate from distinct thalamic nuclei<sup>14</sup>. Therefore, considering the thalamus as a single node overestimates its network relevance and it affects computational analyses. On the other hand, detailed examinations of cortico-subcortical links have been reported using either tractography or functional connectivity, but usually following a seed-based approach and focusing on one structure or area, e.g, for thalamus<sup>14,15</sup>, basal ganglia<sup>15</sup> or brainstem<sup>16</sup>. Motivated by these studies, the central role of some subcortical structures to the brain's communication has been proposed<sup>15</sup> but, so far, no exhaustive investigation has been undertaken to describe the architecture of the brain-wide connectome, nor to detail how cortex, subcortical structures and cerebellum are interconnected at the macroscopic level in the human brain.

Here, we investigated the human structural connectome including the cortex, the cerebellum and nine subcortical structures at the level of interconnected regions of interest (ROIs), as defined from diffusion imaging and tractography<sup>17,18</sup>. With the entire brain parcellated into 718 ROIs, this network presented sufficient resolution to explore the contribution of individual ROIs even within subcortical structures. Our analyses revealed that the brain-wide connectome follows a modular and hierarchi-

<sup>a)</sup> Electronic mail: gorka@Zamora-Lopez.xyz

cal architecture mirroring the one reported for cortico-cortical connectivity<sup>7-9,19-25</sup>, but with significant differences. The human brain is organised into macroscopic network modules, made of intermixed cortical, subcortical and/or cerebellar ROIs thus transcending their individual boundaries. The pathways between these modules are centralised through a communication core (a rich-club) made of cortical and subcortical regions but, importantly, this global rich-club is dominated by subcortical ROIs instead of cortical areas. Surprisingly also, in contrast to previous expectations placing selected structures at the center of the network (e.g., thalamus or basal ganglia), we found all subcortical structures to take part in the rich-club. This is possible because, internally, the ROIs of subcortical structures exhibit heterogeneous network functionalities: some of their ROIs are locally connected while few others are integrated in the global rich-club. Altogether, our study extends the current understanding of the human brain’s organization. It introduces a novel and complementary view by showing how, shaped by white-matter pathways, the brain forms an intermixed network architecture on top of the established division into cortex, subcortex and cerebellum

## RESULTS

Structural connectivity data was obtained via diffusion-weighted imaging for 32 healthy human participants from the Human Connectome Project (HCP), see Ref. [17], and parcellated into 718 regions of interest (ROIs). Of them, 360 correspond to cortical, 233 to subcortical, and 125 to cerebellar cortex (see Ref. [18] for parcellation details). This parcellation provides the internal division of subcortical structures into several ROIs such as bilaterally the nucleus accumbens ( $n=13$ ), brainstem ( $n=47$ ), caudate nuclei ( $n=17$ ), diencephalon ( $n=40$ ), hippocampus ( $n=29$ ), globus pallidus ( $n=20$ ), putamen ( $n=18$ ), thalamus ( $n=38$ ), and amygdala ( $n=11$ ). Tractography data was filtered in order to exclude tracts for which the lack of true anatomical fibers has been reported<sup>5,6,26,27</sup>. Accordingly, the following false positives were filtered out from the connectivity matrix: (i) direct cortico-cerebellar tracks, (ii) direct inter-hemispheric cerebellar connections, and (iii) ipsilateral tracts from the cerebellum to both the thalamus and the brainstem. A population averaged and binary structural adjacency matrix was estimated by applying a distance-aware consensus algorithm. For the rest of the paper, we investigate the properties of this population-level connectivity.

### Network division of the brain-wide structural connectivity

We begin by examining the extent to which the network organization of the structural connectivity reflects the traditional anatomical division of the brain into cor-

tex, subcortex and cerebellum. The density matrix in Fig. 1a shows the average probability of an ROI to connect to other ROIs within (diagonal entries) or outside (extradiagonal entries) their anatomical component. Internally, the subcortex is the densest (32%) followed by the cortex (23%) and the cerebellum (23%). In general, we see that brain regions are 1.82 times more likely connected internally, i.e., to other ROIs in their anatomical component than outside. While this may indicate that the anatomical view into cortex, subcortex and cerebellum is a reasonable division from a network point of view, the lack of direct fibers between cortex and cerebellum magnifies this ratio. In fact, cortical ROIs are equally likely connected with each other as to subcortical ROIs (cor-cor: 0.23; cor-sub: 0.24); and cerebellar ROIs are also highly likely connected to subcortical ones (cer-cer: 0.23; cer-sub: 0.19). This observation begs the question whether this anatomical division is also to be expected as the most representative description from the network perspective, or instead, another system’s level organization may be hidden in the connectivity.

We apply a network community detection algorithm (Leidenalg<sup>28</sup>) to automatically cluster the 718 ROIs based on network properties alone. These methods aim at grouping together nodes that are more densely connected with each other than with the nodes in other groups, by maximizing an intra-/inter-connectivity cost function (e.g., Newman modularity). The optimal solution (resolution parameter  $\gamma = 1.0$ ,  $Q = 0.232$ ; see Supplementary Fig. S1) returned the global network divided into five communities (modules or clusters). The adjacency matrix is shown in Fig. 1b reorganized for this optimal partition, alongside its corresponding density matrix. This network-based division clusters the brain more accurately than the anatomical division. The diagonal entries now display notably larger internal connection probabilities (0.34 – 0.51) and lower cross-modular connection probabilities (0.08 – 0.19). On average, under this network-based division, ROIs are 3.23 times more likely connected internally than to other communities.

The five network communities are made of a mixture of regions surpassing the cortical, subcortical, and cerebellar boundaries (Figs. 1c,d; Supplementary Table 1). Community C1 is made of left and right, ventrally located subcortical (43%) and cerebellar ROIs (57%). As seen, the entire cerebellum is embedded into C1 while the Cortex is not present in C1. Community C2 also comprises cortical (44%) and subcortical (56%) ROIs on both hemispheres. Notably, the cortical regions participating in C2 are located in the frontal and posterior lobes, Fig. 1c. Communities C3 and C4 are predominantly lateralized (right and left, respectively), made of cortical and deeper subcortical ROIs. Finally, community C5 (which is the smallest one) is medially located comprising mainly left and right cortical ROIs (96%) and a few subcortical ROIs (4%). These results evidence that communities C1 to C4 are made of regions that transcend the cortical, subcortical, and cerebellar boundaries; bringing up the question

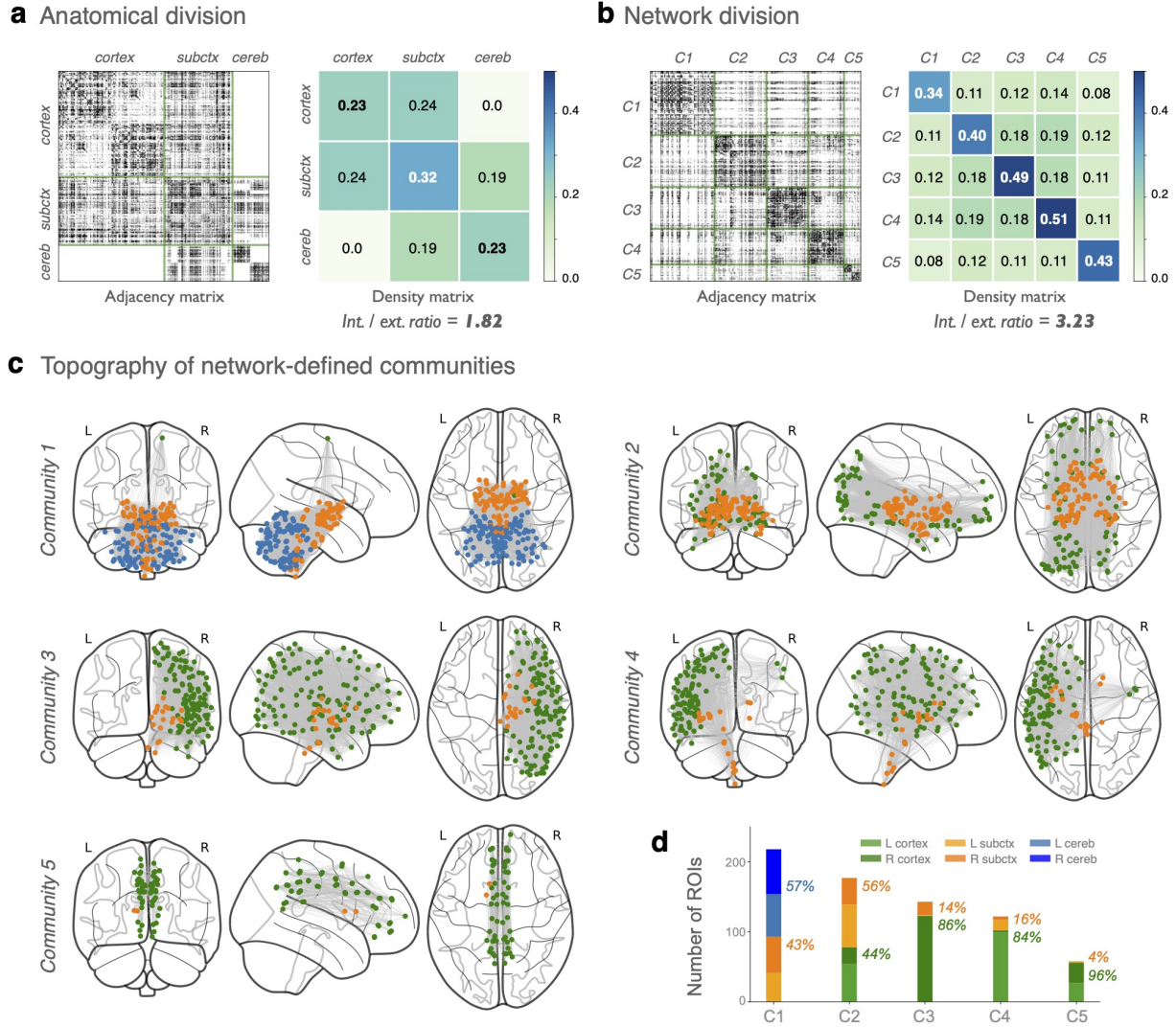


**FIG. 1. Modular organization of the brain-wide connectome.** Structural connectivity matrix and corresponding intra-/inter-modular connection densities for the brain-wide connectivity sorted according **a**, to the traditional anatomical division of the brain into cortex, subcortex and cerebellum, and **b**, to the optimal network division into five communities found by community detection algorithms. The optimal network division shows larger intramodular densities and lower cross-modular connection probabilities than for the anatomical division. **c**, Topographical distribution of the five network communities shows that communities 1-4 vertically stretch over cortical, subcortical, and cerebellar boundaries; communities 3 and 4 are lateralized comprising cortical and subcortical regions and the 5th is made of medially arranged cortical ROIs. **d**, Quantitative composition of the five network communities in terms of cortical, subcortical or cerebellar ROIs, with hemispheric information added to highlight the lateralization of communities 3 and 4.

of which role do the various subcortical structures play in the cohesion of these macroscopic, intermixed network communities.

#### Distribution of subcortical nuclei across network communities

The detailed composition of the five network communities is presented in Fig. 2a. C1 is dominated by the cerebellar cortex, the Brainstem and the Diencephalon, fol-

lowed by contributions from Pallidum and Hippocampus. Community C2 is made of frontal and posterior cortical ROIs, and a mixture of subcortical nuclei: mainly Thalamus, Hippocampus, Accumbens, Caudate and Amygdala, and to a lesser extent, also the Putamen, Diencephalon and Pallidum. Communities C3 and C4 are primarily made of lateralized cortical regions together with some subcortical ROIs from Brainstem, Thalamus, Putamen, Pallidum and Caudate. Finally, C5 is practically a cortical community.

Given that the subcortical structures are smaller than

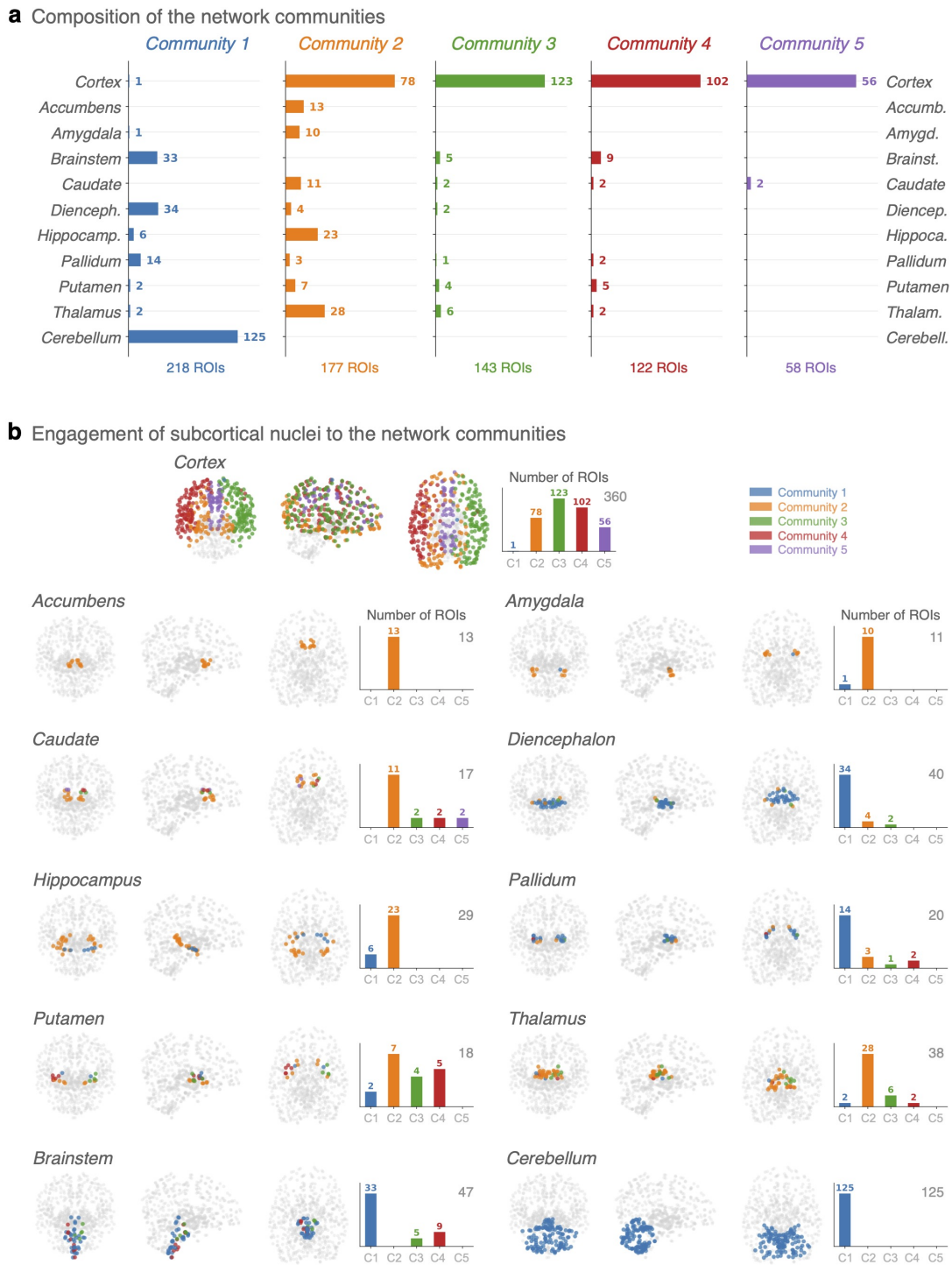


**FIG. 2. Relation between anatomical and optimal network communities.** **a**, Composition of the five optimal network communities in terms of anatomical components, including the division of the subcortex into nine nuclei. Bars indicate the number of ROIs from each anatomical component that was classified into the corresponding network community. Numbers at the bottom summarise the size of the network communities, in total number of ROIs. **b**, Internal division of the nine subcortical structures, the cortex and the cerebellum in terms of the five network-based communities. Topographical maps show that—in most cases except for Accumbens and cerebellum—the ROIs of an anatomical component usually fall into different communities, evidencing an internal distribution of anatomical structures and their participation into different circuits. Bars summarize the number of ROIs that each anatomical component devotes to distinct network communities (C1 – C5). Gray numbers indicate the size (in number of ROIs) of the anatomical components.

the cortex and the cerebellum in number of ROIs, a relative interpretation of these results shall be considered. Hence, we evaluated the fraction of ROIs that each anatomical component contributes to C1 – C5, Fig. 2b. The Putamen is the most segregated subcortical structure, with its 18 ROIs very much distributed among C1 – C4. On the opposite side, the accumbens and the amygdala, both contribute (almost) exclusively to a single community: C2. The rest of nuclei fall in an intermediate situation, with most of their ROIs assigned to one community but few ROIs to other communities.

The involvement of subcortical nuclei into distinct network communities is relevant because it implies that despite their small number of ROIs subcortical structures are internally diverse; with different ROIs potentially participating in different functional circuits. So far, we have analysed the overall division of the brain into network communities and their composition.

### Contribution of individual ROIs to cross-modular connectivity

Next, we investigate how the identified brain-wide communities are interconnected and explore, specifically, the contribution of subcortical connectivity. Network visualization algorithms allow for an approximate representation of a network’s architecture by arranging their nodes according to their relative importance and mutual similarity. The whole-brain connectome is displayed in Fig. 3a (Force Atlas 2 algorithm<sup>29</sup>). In this visualization the network appears centered around the two cortical hemispheres (in green) largely connected to the Thalamus and the Putamen on the one hand, and the Brainstem, the Diencephalon and the Pallidum on the other hand mediating the cortico-cerebellar pathways. The smaller subcortical structures tend to be placed around the periphery, with those contributing mostly to the C2 community (e.g., Accumbens, Amygdala, Hippocampus and the Thalamus; see Fig. 3b) occupying the upper space while the structures more associated to C1 (e.g., Brainstem, Diencephalon and Pallidum; Fig. 3b) are placed towards the bottom, near the Cerebellum.

This spatial separation is reflected in more detail for the subnetworks formed by the individual network communities for C1 and C2, Fig. 3b. The core of C1 is made of substantial interconnectivity between the Cerebellum, the Brainstem (specially its central part) and the Diencephalon. Instead, C2 is governed by strong interconnections between the two cortical hemispheres and a substantial number of connections to the Hippocampus, the Thalamus and the Caudate. C3 and C4 form star-like structures centered on either right or left cortical ROIs.

Although these layouts are informative, they are affected by the size differences between brain regions. Looking at connection probabilities instead of total link numbers, some smaller areas like the Putamen, Amygdala, and Thalamus become more central, highlighting

their key role in connecting different parts of the brain (see Supplementary Figure S2).

We now clarify in more detail the position that every ROI takes within the brain-wide connectome. For that, we map the 718 ROIs based on two parameters<sup>8,30,31</sup>: their degree (i.e., the hubness) and their participation index (which quantifies how evenly the connections of an ROI are distributed across the modules). See Fig. 3c for a schematic description. Hence, the participation of a node depends on how the network was divided into modules in the first place.

Considering the anatomical division (Fig. 3d), cortical and cerebellar ROIs tend to occupy the lower-right and the central sectors of the map, corresponding to nodes with local or intermediate cross-modular connections. The reason is the absence of direct connections between Cerebellum and Cortex. Thus, under this anatomical view, cortical and cerebellar ROIs span their connections, at most, among two of the three modules (i.e., either cortex and subcortex, or cerebellum and subcortex) and thus attain a maximal participation index of 0.5. On the other hand, several subcortical ROIs occupy the upper-right sector of the map which is characteristic of supramodal hubs (e.g., purple diamond in Fig. 3c). Importantly, this indicates that at the systems’ level, the brain-wide communication is primarily sustained by subcortical regions.

Considering the network-based division (Fig. 3e), the 718 ROIs distribute along the diagonal axis of the 2D map (top-left panel), which is a signature of a modular and hierarchical organization<sup>8,31,32</sup>. Disentangling the results individually by anatomical component, the ROIs of the cortex display a wider variety of roles as compared to the results under the anatomical division. It now includes some hubs of high participation (up to 0.86). On the contrary, cerebellar ROIs still fall into the lower-left sectors of the map. Given that C3 – C5 are mainly made of cortical regions and the absence of direct cortico-cerebellar fibers, cerebellar ROIs span their connections mainly among C1 and C2. For the subcortical structures, the results show a rich variety of connectivity roles. For example, all ROIs of the Accumbens ( $n=13$ ) and the Amygdala ( $n=11$ ) were classified into C2, but some of their ROIs take a central role with large degree and high participation. The Caudate ( $n=17$ ) and the Putamen ( $n=18$ ) are two other small nuclei that contain ROIs with high degree and participation, although in this case it is more expected, given that they contribute to C2 – C5 and C1 – C4 respectively, Fig. 2.

Altogether, these results show that subcortical structures are internally heterogeneous. Within each structure, their ROIs occupy different positions in the network architecture thus playing differential roles for the cross-modular communication. Some ROIs form mostly local connections (characterised by low degree and participation) and others span their connections across multiple communities (large degree and participation) becoming crucial for the centralization of the brain-wide pathways.



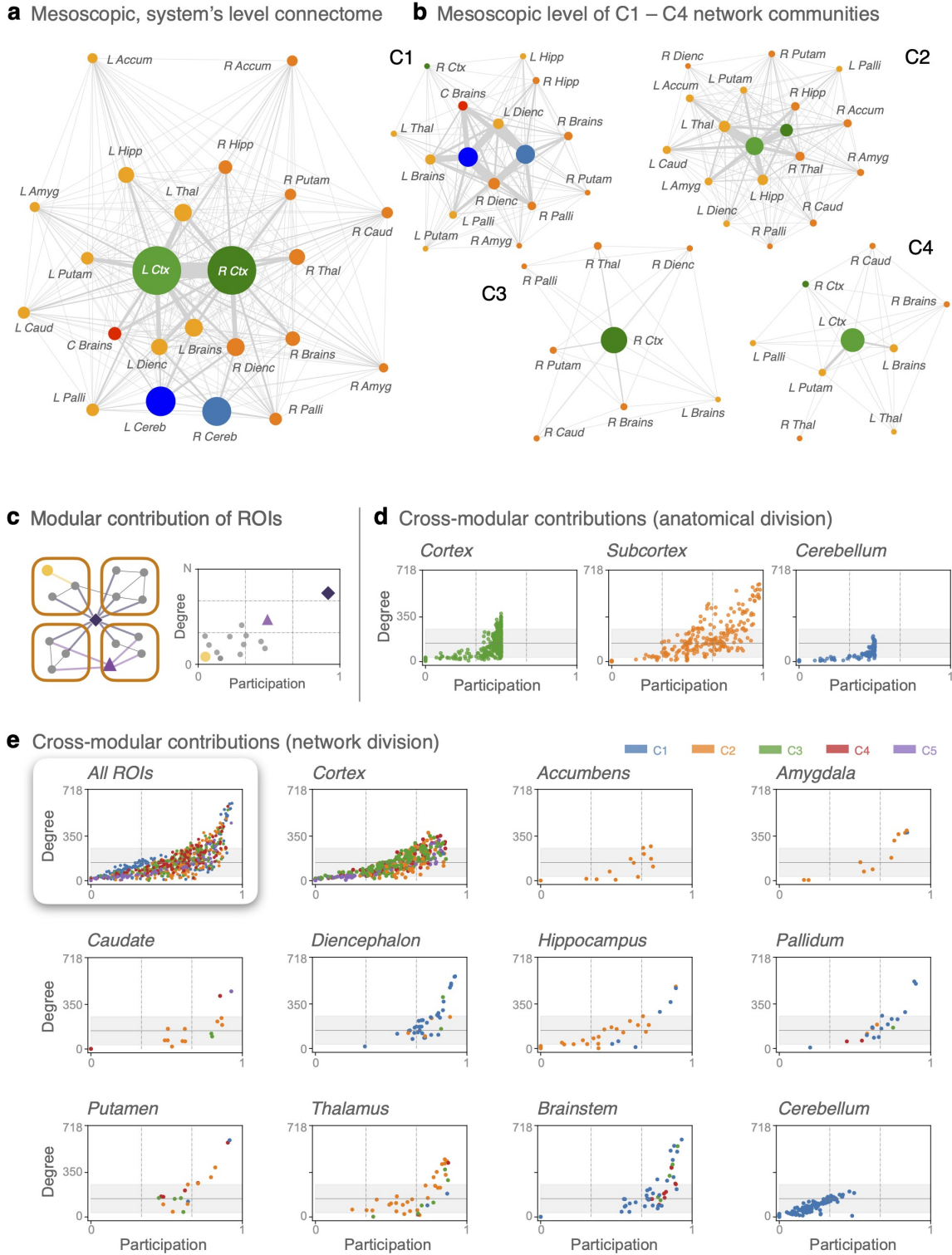


**FIG. 3. Contribution of anatomical components to cross-modular connectivity.** **a, b**, Visualization of the structural connectivity at the level of anatomical components comprising the cortex, the cerebellum and nine subcortical structures; **a** for the brain-wide network and **b** the subnetworks representing network communities C1 to C4. Link widths reflect the number of ROIs connected within the two components. **c**, Illustration of different roles that nodes can play within a modular and hierarchical network, and their characterization. Nodes can be either locally connected inside a module (yellow dot), be well rooted in a community but share connections to other communities (purple triangle), or uniformly participate over all communities (dark purple diamond). **d**, Mapping of the roles of all the ROIs, considering the network is divided into cortex, subcortex and cerebellum. For visual clarity, the 718 ROIs are presented in three separate maps for cortical, subcortical and cerebellar regions. The solid horizontal lines represent the average node degree and gray shadows the range for one standard deviation. **e**, Mapping of the roles for all the ROIs, considering the network is divided into the five network communities. Top left panel shows all the 718 ROIs on a single map. The remaining panels show the same results but individually for the ROIs of each of the 11 anatomical components studied.

### Subcortical hubs dominate the communication core of the brain-wide connectome

The results of Fig. 3 highlighted the presence of hub ROIs in diverse anatomical structures. We now inquire whether these centralizing hubs form additional structures that help elucidate the global network architecture. Focusing on the distribution of the 100 most connected ROIs, Fig. 4a, it shows that the leading hubs are mainly subcortical (60%), followed by cortical hubs (40%) and no presence of cerebellar ROIs among the top 100. A closer look at the subcortex (middle panel) also confirms that the subcortical hubs are very much distributed among the different subcortical structures (regardless of their size) and thus, no single subcortical structure can be considered responsible for the centralization of the communication pathways. This distribution of hub regions is more evenly observed in the light of the network-based division, with the communities C1 – C4 containing 19% – 29% of the leading hubs each.

This resonates with previous observations, where cortical hubs were found to be spatially dispersed instead of forming a localized anatomical structure of their own<sup>7–9</sup>. And this, despite that cortical hubs were found to be densely interconnected, forming a communication core, also known as a rich-club supracommunity, Fig. 4b (left panel). Here too, we identify clear evidence that the brain-wide hubs form a rich-club suprastructure. By iteratively removing the ROIs with less connections, the internal density of the remaining subnetwork (made of the ROIs with larger degree) rapidly increases, Fig. 4b (right panel). There are 170 ROIs with degree  $k > 208$ , forming a core of density 0.8. In comparison, this is 56% denser than C4, which is the densest (0.51) of the network communities identified. The 100 leading hubs displayed in Fig. 4a form a rich-club with an approximate density of 0.93; see their topographical location in Fig. 4c (right). As the threshold is increased, the number of hubs in the rich-club decreases. Mainly at the expense of cortical hubs, emphasizing the central role of subcortical hubs in the brain-wide network, Fig. 4c (lower panel) and Fig. 4d (right).

The analysis performed here shows that, at the system's level, the connectivity of the entire brain follows similar organization principles as those observed for the cortico-cortical connectivity alone: it is structured into a handful of network modules with the cross-modular connectivity centralized via hub ROIs, which form a spatially delocalized supramodule at the core, Fig. 4e. However, in this global case, we found that it is the subcortical ROIs—instead of cortical areas—which dominate the communication core of the network, while the cerebellum is excluded from the rich-club, Fig. 4e (left panel). Particularly relevant is the fact that no single subcortical structure centralizes the global pathways, but instead, subcortical hubs appear distributed across the different structures. This is further highlighted from the viewpoint of the network-based division, with the rich-club

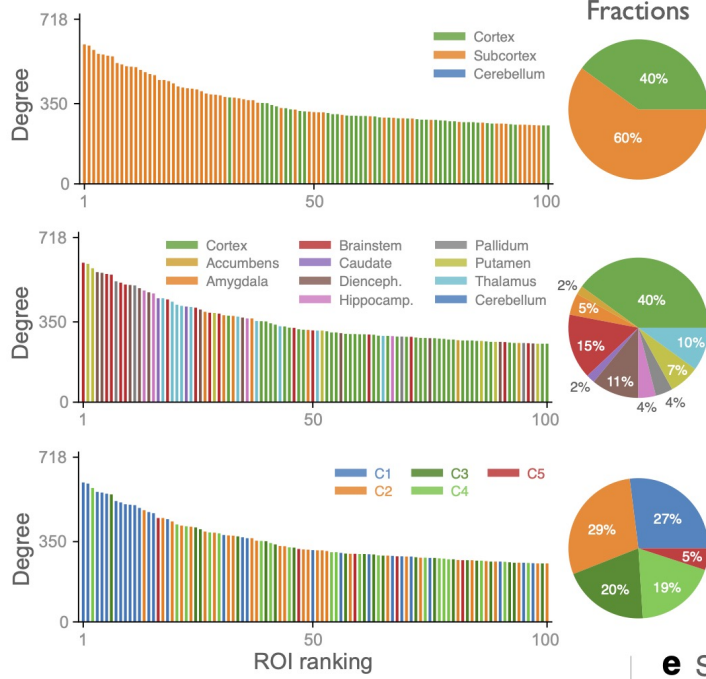
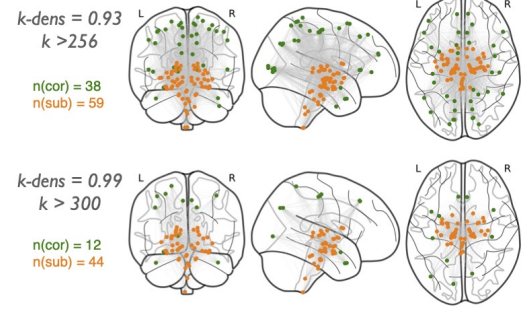
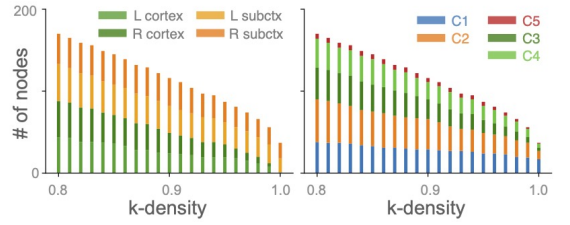
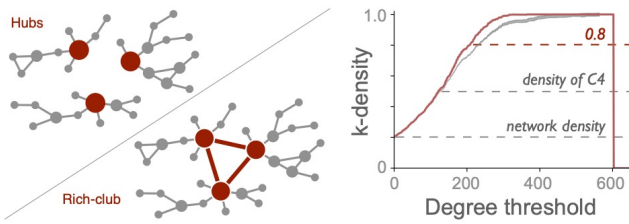
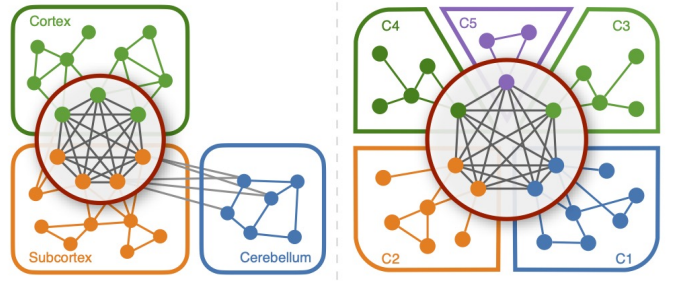
hubs evenly dispersed among the network communities.

### Global integration and segregation in the brain-wide connectome

We conclude by exploring the functional implications of the brain-wide architecture revealed so far and depicted in Fig. 4e. For that, we examine its role in balancing integration and segregation, and its vulnerability to targeted lesions. We evaluate integration and segregation following an in-silico perturbative approach based on network responses to external stimuli<sup>7</sup>. This approach accounts for the influence of brain regions on each other through all possible pathways, beyond one-to-one connections<sup>33,34</sup>.

Integration is defined as the joint response of a group of hubs to stimuli applied at the rest of the network, see Fig. 5a for an illustration. For example, taking the thirty leading hubs, either globally or locally per module, the integration capacity of subcortical hubs is clearly larger than that of cortical and cerebellar hubs, Fig. 5b (top). This uneven integration capacity is maintained when evaluated for groups of hubs of increasing size, by sequentially adding one hub at a time, Fig. 5c (top). The integration capacity of subcortical hubs (orange curve) is the largest across all group sizes—practically explaining the integration capacity of the global hubs (black curve), followed by that of cortical hubs (green curve). The integration capacity of the cerebellar hubs (blue) is very small in all cases. From the viewpoint of the network division, the integration capacity of hubs—selected by community—is more evenly distributed, Figs. 5b,c (bottom). Although C1 displays a larger integration than the rest and integration of C5 is clearly smaller. The integration of local hubs of the C1 – C4 communities remain close to each other regardless of the number of hubs taken, Fig. 5c (bottom).

We define segregation as the loss of influence between communities, after a number of hubs has been lesioned<sup>7</sup>, see Fig. 5d for illustration. For quantification, the influence of one community on another is first measured in the original (healthy) network. Then, a number of hubs is lesioned and the cross-modular influences are measured again to evaluate the relative difference, from healthy to lesioned. When the thirty leading global hubs are lesioned, the segregation suffered by the network is drastic: 48–68% of communication is lost between the three anatomical communities and 38–63% among the network-based ones, Fig. 5e. The largest loss occurs between cortex and cerebellum (68%), given the circumstance that subcortical pathways are crucial for cortico-cerebellar communication. On the same order (63%) is the loss of communication incurred between C1 and C2 network communities. The total segregation after lesion of the 30 leading global hubs is of 50%, Fig. 5f (black bars). This level of segregation is striking taking into account that thirty hubs represent only 4% of all the ROIs.

**a** Origin of the leading hubs**c** Topography of the global rich-club**d** Consistency of the rich-club**b** Rich-club organization**e** Schematic architecture of the brain-wide network

**FIG. 4. Hierarchical centralization of cross-modular connectivity.** **a**, Analysis of the 100 lead hub ROIs of the brain-wide network. Bar panels display their degree—sorted in decreasing order—with the bars colored according to the community to which the ROI belongs, in the three different divisions. Pie charts show the fraction of leading hubs among the subsequent communities. **b**, Evidence for a rich-club supraorganization among the leading hubs. Left panel, conceptual illustration of a rich-club, formed when the leading hubs are densely connected with each other. Right panel, evolution of the link density for the subnetworks formed by ROIs with degree larger than  $k$  (nodes with degree smaller than  $k$  are removed), for all possible thresholds of  $k = 0, 1, \dots, 718$ . Red curve is the evolution for the brain-wide network, gray curve is for degree-conserving randomized samples (100 independent realizations each point). The threshold for  $k = 0$  represents the entire network, thus, the curves begin from a density of 0.2. Their monotonic increase up to a density of 1.0 evidences that the leading hubs eventually form an all-to-all connected core, centralizing the communication pathways. **c**, Topographical location of the rich-club hubs and their mutual links, for two different density thresholds: at  $k > 256$  (subgraph density of 0.93) and  $k > 300$  (subgraph density of 0.99). Cortical ROIs are shown as green dots and subcortical ROIs in orange. **d**, The composition of the rich-club at different levels of internal density, from 0.8 to 1.0 (degree thresholds,  $k \geq 208$  to  $k = 365$ ), displayed for the anatomical (left or right cortex, subcortex, cerebellum) and the network divisions (C1 – C5). Bars indicate the number of ROI hubs forming the rich-club at each density level, and how many of them belong to the different anatomical or network communities. **e**, Schematic representation of the modular and hierarchical organization of the brain-wide structural connectivity, in the light of either the anatomical or the optimal network divisions.

A comparable lesion of thirty ROIs chosen at random would only imply a segregation of 13% for either the anatomical or the network communities (dashed lines). Selecting the hubs per community, the largest segregation (50%) occurs when subcortical hubs are lesioned

(top panel, orange bar), which is twice the segregation incurred by the lesion of cortical hubs (24%, green bar). Selecting hubs per network community, Fig. 5f (bottom), again we identify a more even segregation for targeted C1 – C4 hub lesions, as for their integration capacity.



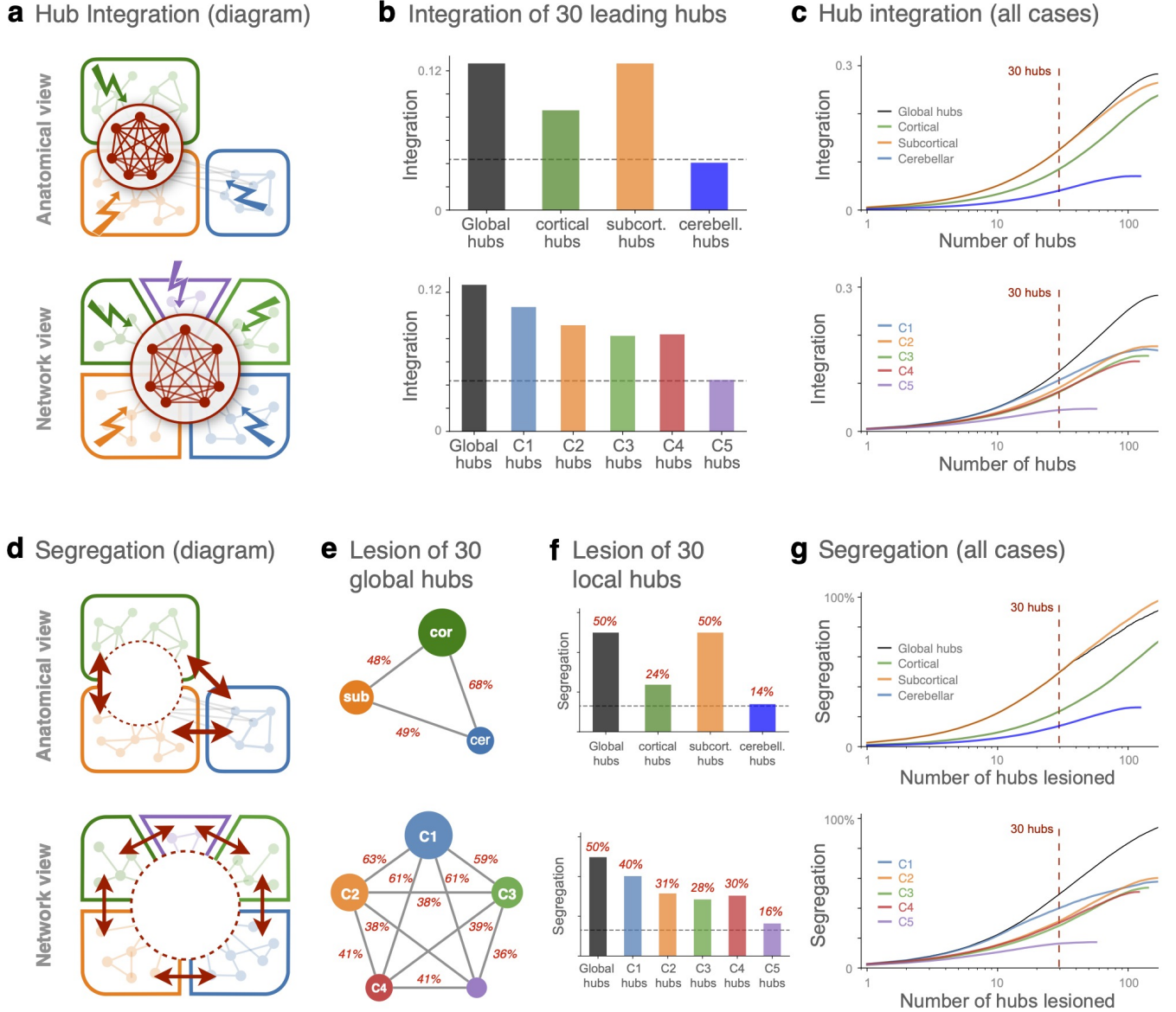


FIG. 5. **a**, Schematic illustration of the integration capacity metric for a set of ROIs, in this case, the network hubs. Illustration for both the anatomical or the network divisions. Integration is defined as the joint response of a group of ROIs (the hubs), to stimuli applied in all other ROIs. **b**, Integration capacity of the 30 leading hubs, chosen from the global ranking (black bars) or chosen from the local ranking at each community (colored bars). Top, for the anatomical division into cortex, subcortex, and cerebellum; bottom, for the leading hubs within the network communities C1 – C5. Dashed lines indicate the average integration capacity of 30 randomly chosen ROIs, regardless of their hubness (average of 100 realizations). **c**, Integration capacity of the  $n$  leading hubs, with  $n$  from 1 to 170. Black lines, choosing hubs from their global ranking and, colored lines, choosing the hubs of a given community, see Fig. 4a (top and bottom). Notice that the sizes of cerebellum, C3, C4 and C5 are smaller than 170, thus, their last points reflect the integration capacity of the entire community. **d**, Schematic representation of the modular segregation metric, in both the anatomical and the network divisions. Segregation is defined as the conditional loss of communication between modules, given that a set of  $n$  ROIs has been lesioned. In this case, a set of hubs is lesioned. **e**, Loss of communication between the modules after the leading 30 global hubs have been lesioned. Numbers indicate the loss between each pair of modules. **f**, Segregation suffered by the network after lesion of the 30 leading hubs, selected from the global ranking (black bars) or locally selected within a community (colored bars). Dashed lines indicate the average modular segregation after 30 randomly chosen ROIs are lesioned (average of 100 realizations). **g**, Modular segregation suffered by the network after the  $n$  leading hubs have been lesioned, with  $n$  from 1 to 170. Black lines, choosing hubs from their global ranking and, colored lines, choosing them within each community. Notice that the sizes of cerebellum, C3, C4 and C5 are smaller than 170, thus, their last points reflect the segregation of the network after the entire community has been lesioned.

Cumulative lesion of ROIs, from largest to smallest degree, confirms that subcortical lesions are the most disruptive for the communication in the network, Fig. 5f (top). For sizes up to 100 ROIs, the lesion of subcortical hubs causes 60 – 140% larger segregation than the lesion of cortical hubs alone. However, from the viewpoint of the network-based communities (bottom), local lesions to ROIs within the C1 – C4 communities lead to similar levels of segregation.

These results confirm the central importance of subcortical regions to sustain brain-wide communication. Also, they show that the modular and hierarchical network organization defined by the connectivity (Fig. 4e, right) constitutes a more balanced distribution of the brain into large-scale circuits.

## DISCUSSION

The division of the brain into cortex, subcortical structures and cerebellum is an essential notion of the brain's organization, rooted in their different cytoarchitecture, cellular composition and evolution. However, there is more to brain's organization than meets the eye, hidden in the complex manner that white matter shapes the pathways between distant regions, and only discernible through suitable network analyses. Despite the tight functional interdependencies between cortex, subcortex and cerebellum, to date, a detailed description of the brain-wide communication network they form remains undisclosed. We employed high-quality tractography data from the Human Connectome Project to construct a structural connectome of the entire human brain (at the level of interconnected regions of interest) as a first step towards uncovering the principles of how cortex, subcortex and cerebellum are integrated.

First, we found that the brain is organized into network modules of mixed cortical, subcortical and/or cerebellar regions (Figs. 1 and 2). This mixture may facilitate the brain to collectively orchestrate a spectrum of functions ranging from basic motor control up to complex higher-order cognition. Second, we identified that the communication pathways between these modules are centralised through a number of highly connected ROIs forming a rich-club. Importantly, this rich-club is dominated by subcortical regions: 60% of the leading hubs are subcortical (Fig. 4) and their in-silico lesions greatly disrupt the communication throughout the network, significantly more than cortical lesions alone (Fig. 5e,f). Last, but not least, we found that subcortical structures are internally heterogeneous, with their ROIs displaying diverse local and global connectivity profiles and thus playing different roles in the network architecture (Fig. 3e). More so, the subcortical hubs are spatially segregated, meaning that all subcortical structures engage in the rich-club instead of one structure (e.g., thalamus or basal ganglia) centralising the communication pathways. Altogether, our results complement the traditional view of the large-

scale organization of the human brain and invite to question the prevalent cortico-centric notion that regards subcortical structures and cerebellum as 'mere' supporters of cortical function. Instead, our results reveal a network architecture centered at the subcortex but made of transversal pathways.

## Intermixed modular organization

Subcortical regions are known to heavily interlink with the cortex via a multitude of pathways, for instance, the amygdala<sup>35</sup>, the hippocampus<sup>36,37</sup>, the basal ganglia<sup>38,39</sup>, the superior colliculus<sup>40</sup>, and the thalamus<sup>39,41,42</sup>. Also, the cerebellum is linked to the cortex via the cortico-ponto-cerebellar and the cerebello-thalamo-cortical pathways<sup>5,6,26,27</sup>. The network communities here identified robustly underscore this mixed interconnectivity, as they show larger internal connection densities than separately the cortex, subcortex, and cerebellum but range over their boundaries, Fig. 1a,b.

The five communities identified contain ROIs associated with low-level sensory and motor processing, emotion, and high-level cognition including memory, attention, executive control, language and social cognition. Superimposed upon this extensive functional diversity, each module exhibits functional biases. Community C1 largely comprises of cerebellar and subcortical structures (mainly Diencephalon, brainstem and Pallidum), prominently featuring ROIs related to visceral or autonomic signal processing, emotion and motor control. C2 comprises primarily of anterior and posterior cortical regions together with subcortical structures (mostly thalamus, hippocampus, accumbens, caudate and amygdala), featuring memory-related ROIs. C3 and C4 are cortically dominated and show hemispheric lateralization. In line with prior reports on functional localization, the left-hemispheric community (C4) comprises more ROIs associated with language<sup>43,44</sup> and attention<sup>45</sup> than the right-hemispheric community (C3) whereas the right-hemispheric community comprises more ROIs associated with social cognition<sup>46,47</sup>. However, C5 is primarily made of medial cortical areas; it exhibits the largest proportion of ROIs related to social cognition and to internally oriented cognition.

## Composition and function of the subcortical core

The existence and function of multimodal (transmodal) "convergence zones" has long been debated given the need of the brain to integrate "somewhere" sensory information from different modalities, initially processed by specialised regions<sup>48–52</sup>. Early structural connectivity data showed the presence of highly connected nodes (network hubs) in the neural system of the *C. Elegans*<sup>53–55</sup> and in the brains of macaques, cats and humans based primarily on cortico-cortical connectivity<sup>19,20,34,56,57</sup>. It

was soon identified that these network hubs were not only largely connected throughout sensory modalities, but were also densely interconnected with each other forming a higher hierarchical supramodule: a ‘rich-club’. A generalised assumption was drawn that such a rich-club may provide the structural backbone for centralised but distributed processing<sup>7,9</sup> previously postulated, for example, by the Global Workspace Theory<sup>58,59</sup>.

The importance of subcortical hubs has been recognised by studies focusing on specific structures, e.g. see Refs. [15, 16, and 60]. Our results extend these reports by finding a rich-club core at the whole-brain scale which, crucially, is dominated by subcortical regions (Fig. 4a,c,d). Following our in-silico analyses of the propagation of stimuli, subcortical hubs emerged as the most integrative nodes within the global connectome (Fig. 5b,c) and their lesions led to significantly larger disruption of network communication than lesions of cortical or cerebellar hubs (Fig. 5f,g). These analyses thus contribute to a better understanding of clinical evidence that subcortical lesions are more likely to cause coma than cortical lesions<sup>1,61,62</sup>, and that patients with subcortical lesions are less likely to recover consciousness than patients with cortical damage<sup>61,63,64</sup>.

The central role of the subcortical hubs for the brain-wide communication is remarkable considering that the subcortex only houses 0.8% of the neurons in the brain and 8% of the total brain mass<sup>17</sup>. This disparity highlights the subcortical component of the global rich-club as a critical network bottleneck where widespread neural signals converge onto a rather small number of neurons whose activity is then broadcasted globally. Moreover, given the observed heterogeneity in network position among subcortical ROIs. Specifically, while individual subcortical structures harbor ROIs that serve as critical hubs within the brain-wide network, these same structures also contain ROIs exhibiting markedly lower connectivity and restricted inter-community integration. These observations raise compelling questions about the specific computations the subcortical structures and rich-club may perform. This intra-structural coexistence of highly integrative hubs alongside more segregated subregions may reflect a functional specialization, potentially delineating roles in localized information processing alongside broader network communication. Collectively, these observations underscore the imperative of considering the global connectome, and the topological position of brain regions within it, to achieve a more comprehensive understanding of their functional contributions.

## Limitations and Outlook

The construction of structural connectomes based on diffusion imaging are inherently constrained by the spatial resolution and technical capabilities of the equipment and methodology. The occurrence of false-negative and false-positive connections is a common issue when

estimating structural connectivity from diffusion imaging. To mitigate this, the connectivity matrices were thresholded to preserve the original distribution of connection lengths, thus maintaining long-range fibers. Also, based on established anatomical knowledge direct cortico-cerebellar tracts, interhemispheric cerebellar connections, and ipsilateral cerebellar connections to the thalamus and brainstem were excluded. Some recent studies have investigated the structural connectivity between cortex and subcortex with a notable level of detail<sup>14,40,65,66</sup>. However, these works focused on selected subcortical structures. While this choice allowed high specificity of connections, they lack of the systems’ level viewpoint that we aimed at the present study, e.g., missing on the internal heterogeneity of connection profiles within these structure or the complex composition of the rich-club.

Obtaining both a high-level of detail and an overarching structural connectome is currently a major challenge for diffusion imaging. But the onset of ultra-high field imaging?scanning ex-vivo at high Teslas?will soon allow the description of the entire human structural connectivity at an unprecedented level of resolution<sup>67,68</sup>. Together with the recent release of the whole-brain wiring map of fruit fly<sup>69,70</sup>, we are about to undergo a breathtaking time to not only explore the brain’s organization, but also to inquire about its evolutionary mechanisms via comparative connectomics<sup>24,25</sup>. Despite the methodological precautions of this study, our findings represent an initial map and first wiring principles towards a comprehensive description of the brain’s overall architecture.

## METHODS

### fMRI data acquisition

**Subjects and dataset.** In this work we employed the connectivity dataset from Ref. [18], which based on the Human Connectome Project (HCP) with 32 participants (“MGH HCP Adult Diffusion,” 16 females, 16 males) collected at the Massachusetts General Hospital<sup>71</sup>.

**Data Acquisition.** The whole-brain echo-planar imaging was conducted with a modified 3T Siemens Skyra (Connectome Skyra) system with a 32 channel head coil applying a time to repetition (TR)=720ms, time to echo (TE)=33.1ms, flip angle=52, bandwidth=2,290 Hz/pixel, in-plane field of view (FOV)=208 × 180mm, 72 slices, and 2.0mm isotropic voxels, with a multi-band acceleration factor of 8, Ref. [72]. For more details see Ref. [18].

**Functional networks and subcortical / cerebellar ROI assignment.** The functional network calculation and the subcortical / cerebellar ROI assignment was previously performed by Ref. [18]. In detail, subject-specific functional connectivity matrices were calculated by correlating the individual cortical BOLD signals with

Pearson correlation. By averaging across all subject matrices, a group-averaged functional connectivity (FC) matrix was constructed. Cortical resting-state functional networks were obtained by applying the Louvain algorithm to this group-averaged functional connectivity matrix<sup>73</sup>. Next, subject-wise FC matrices indicating the correlation between the 360 cortical ROIs and 31870 subcortical / cerebellar grayordinates spanning over the entire CIFTI space were calculated and averaged to obtain a group-representative cortical-subcortical / cerebellar FC matrix. These grayordinates were assigned to cortical functional networks with the highest correlation and merged together based on this partition. At the same time, the parcels were constrained to major subcortical structures as determined by Freesurfer, thus adhering to the general subcortical anatomy. This resulted in a partition of 233 subcortical and 125 cerebellar ROIs based on the detected cortical functional networks.

### Whole-brain structural network construction

**Structural scan.** The structural connectomes of the participants were averaged to generate a representative connectome. For the DWI a high-quality protocol was applied (i.e. b-value of 10,000 s/mm<sup>2</sup>, high-angular resolution, and a multi-slice approach). The data are publicly included within the Lead-DBS software package and were already preprocessed<sup>74,75</sup>. A generalised q-sampling imaging algorithm (DSI Studio; <http://dsi-studio.labsolver.org>) was used for the data processing. SPM 12 was used to segment and co-register the data. 200 000 fibres were examined for each participant using Gibbs' tracking approach<sup>76</sup> and being restricted by a co-registered white-matter mask. The fibres were standardised into MNI space via DARTEL transforms<sup>77,78</sup>. The cortex was parcelled into 360 regions (180 per hemisphere) according to Ref. [79].

**Filtering false-positive structural connections.** The cortex and cerebellum are contra-laterally connected via the cortico-ponto-cerebellar (CPC) and the cerebello-thalamo-cortical (CTC) pathways<sup>5,6,26,27</sup>. To only display direct anatomical connections, initial cortical-cerebellar connections were filtered as diffusion imaging cannot distinguish between direct and indirect pathways. This resulted in the filtering of 8.3% of initial connections. Moreover, ipsilateral connections between the cerebellum and the brainstem (pons) / thalamus (total of 2.0% of initial connections) and direct inter-hemispheric cerebellar connections (as the cerebellar hemispheres are indirectly connected via the vermis<sup>27</sup>; 2.6% of initial connections) were filtered.

**Binarization of the population-level connectivity matrix.** The individual SC matrices for the 32 participants were averaged into one population brain-wide structural connectivity network, represented as the weighted global connectivity matrix  $W$  of  $718 \times 718$  (ROIs). To perform a graph analysis, commonly  $W$  is

binarised by applying a hard threshold  $\theta$  such that only the connections with a weight larger than  $\theta$  are conserved. That is, the binary adjacency matrix  $A$  is defined as  $A_{ij} = 1$  if  $W_{ij} > \theta$ , and  $A_{ij} = 0$  if  $W_{ij} < \theta$ . The value of  $\theta$  then controls the final number (density) of connections. This typical hard thresholding leads to a bias. Since one of the limitations of tractography is that it overestimates shorter connections, the hard thresholding favours short-range links in detriment of long-range ones<sup>80,81</sup>. Nevertheless, the existence of long-range connections has been shown in tract-tracing studies<sup>82,83</sup> and are thought to serve important functional roles<sup>81</sup> as these connections cause a higher metabolic cost for the organism<sup>84</sup>. To threshold the weighted matrix  $W$  while also maintaining long-range connections, we introduce the "relative weight distance-dependent" (RWDD) thresholding. The goal of RWDD is to conserve the original distribution of connection lengths by performing an adaptive threshold such that  $\theta = \theta_d$  depends on the distance  $d(i, j)$  between two ROIs. Here,  $d(i, j)$  will represent the Euclidean distance between the centers of mass of two ROIs  $i$  and  $j$ , but it could be replaced by the fiber-length of the tracts when this information is available.

All links of the initial SC matrix were binned into  $N$  bins according to their length. This information is taken from a distance matrix, representing the distances between all nodes. Thus, each bin contains similarly long connections. Next, the relative weight of each bin is calculated, i.e., the number of connections in the bin compared to all connections in the initial SC matrix. Finally, the bins are reduced such that this relative weight is maintained and the number of final links for the thresholded SC matrix is reached. While doing so, only the strongest connections of the bins are retained.

Consequently, the RWDD thresholding was applied with a target density of 0.2. While targeting for a low density to reduce false-positive connections, unconnected components (i.e., ROIs with no connections to other ROIs) could be created. To account for this, strong connections of otherwise unconnected ROIs were being kept. If an ROI had the risk of becoming disconnected, links with a weight of 1.8 standard deviations above the mean were kept. This resulted in 12 additional links conserved which would initially violate the RWDD thresholding criteria.

### Network analyses

Several network measures were applied to characterise the brain-wide structural connectome here investigated.

The *density*  $\rho(G)$  of a network  $G$ , is the fraction between the number of links  $L$  present and the maximum possible number of links  $L_{max} = \frac{1}{2}N(N-1)$ , where  $N$  is the number of ROIs in a network. Similarly, the connection densities between modules in a network (e.g., cortex and subcortex) were calculated as the fraction of links  $L_{\alpha\beta}$  present between modules  $\alpha$  and  $\beta$ , and the maximum

possible number of links between them  $N_\alpha N_\beta$  where  $N_\alpha$  and  $N_\beta$  are the number of nodes in each module.

The *degree* of a node  $k_i$  is the number of nodes to which node  $i$  connects.

The *participation coefficient*  $p_i$  is a measure how a node distributes its links among modules<sup>30</sup>. Here we applied the normalised participation index defined in Ref. [31], as it takes into account the relative sizes of communities. The participation of node  $i$ , in a network divided into  $M$  modules is defined as:

$$p_i = 1 - \frac{M}{\sqrt{M-1}} \sigma(P_i), \quad (1)$$

where  $P_i$  is the participation vector of node indicating the probability that node  $i$  belongs to each of the  $M$  modules, and  $\sigma(P_i)$  is the standard deviation of the participation vector. When  $\sigma(P_i) = 0$  indicates that the node has only links within the own community, whereas a value of  $\sigma(P_i) = 1$  indicates the node is equally likely connected to all the modules in the network.

A *Rich-club* consists of supramodule of highly interconnected hubs<sup>85</sup>. The quantitative definition of a rich-club is an undisclosed problem since, in most cases, no unique set of nodes can be strictly defined as ‘the rich-club’. Instead, the presence or not of a rich-club is discriminated evaluating the  $k$ -density  $\Phi(k')$  function, which is the internal link density between the nodes with  $k$  larger than a given  $k'$  such that:

$$\Phi(k') = \frac{L_{k'}}{N_{k'}(N_{k'} - 1)}, \quad (2)$$

where  $N_{k'}$  is the number of nodes with degree  $k > k'$  and  $L_{k'}$  is the number of links between them. Iteratively computing  $\Phi(k')$  for  $k' = 0, 1, 2, \dots, k_{max}$ , if the function monotonically increases, then we can assure a rich-club is present in the network. To perform a comprehensive analysis, instead of taking a single threshold, we studied the resulting rich-club organization for different thresholds in the range of  $\Phi(k') = [0.8, 1.0]$ . For comparative purposes,  $k$ -density was also estimated out of an ensemble of 100 random graphs conserving the degree distribution, using the link-switching method<sup>86</sup>.

**Community detection.** We applied the Leiden community detection algorithm<sup>28</sup> to the brain-wide structural matrix. To account for different resolution parameters, we first applied the ‘RB’ null-model<sup>87</sup>. For each step of size of 0.05 in the range of  $\gamma \in [0.6, 1.4]$ , the algorithm was run 100 times and the partition with the highest quality value selected. Finally, the partition of this set with the highest modularity index<sup>88</sup> was chosen, see Supplementary Fig. S1.

### Measuring integration and segregation

Integration and segregation of the brain-wide network were estimated using the definitions introduced in<sup>7</sup>. This

approach accounts for the integration capacity of a group of nodes and for the segregation (loss of communication) suffered by a network, after selected nodes have been lesioned. These are defined in general and can be evaluated under different dynamical or propagation models. For the exploratory purposes of the present study, we employed an analytical account of the dynamical influence that one node  $j$  exerts over another  $i$ , by measuring the network response measured at  $i$  to an stimulus applied at  $j$ .

**Stimulus-response matrices** . Assuming the dynamics of the network (represented by its connectivity matrix  $A$ ) are governed by a continuous leaky-cascade (a multivariate autoregressive process), the temporal evolution of the system is given by:

$$\dot{\mathbf{x}} = -\frac{\mathbf{x}}{\tau} + A\mathbf{x}, \quad (3)$$

where  $\mathbf{x}(t) = [x_1(t), x_2(t), x_3(t), \dots, x_N(t)]^T$  is the (column) vector of the temporal states  $x_i(t)$  for nodes  $i = 1, 2, \dots, N$ , and  $\tau$  is a leakage or a dissipation time-constant. In this linear system, the temporal response  $R_{ij}(t)$  of node  $i$  at times  $t > 0$  to a unit stimulus applied at node  $j$ , at time  $t = 0$ , can be analytically estimated<sup>33,34</sup>. Assuming that initially all nodes receive a unit stimulus, the temporal response matrix is obtained as:

$$R(t) = e^{Jt} - e^{J^0 t}, \quad (4)$$

where  $J_{ij} = -\frac{\delta_{ij}}{\tau} + A_{ij}$  is the Jacobian matrix of the linear dynamical system and  $J_{ij}^0 = -\frac{\delta_{ij}}{\tau}$  corresponds to the trivial leakage through a node, due to a perturbation applied on itself. This pair-wise response encompasses all network effects from  $j$  to  $i$  acting at different time scales along all recurrent paths of different lengths. If  $\lambda_{max}$  is the largest eigenvalue of the connectivity matrix  $A$ , the responses will converge to zero after a transient response only if  $\tau < 1/\lambda_{max}$ . Otherwise, if  $\tau > 1/\lambda_{max}$ , the system diverges and so do the responses measured. For the calculations here, we considered  $\tau = 0.5 (1/\lambda_{max})$ .

So far,  $R_{ij}(t)$  represents the temporal evolution of the responses. For the estimation of integration and segregation, the total response of node  $j$  to  $i$  were obtained as the accumulated response over time, by computing its integral over time (or area-under-the-curve from  $t = 0$  to  $t = \infty$ ),

$$R_{ij} = \int_0^\infty R_{ij}(t) dt. \quad (5)$$

In the following, we will refer this  $N \times N$  matrix  $R$  as the ‘pair-wise response matrix’.

**Integration capacity.** Here, we define integration not as a global property of a network, but as the capacity of one node, or of a set of selected nodes, to integrate the information in the network<sup>7</sup>. Let  $X$  be the set of all nodes in a network and  $H \subset X$  a subset of arbitrarily chosen



nodes. Then, the integration capacity  $I(H)$  is defined as the joint response by the nodes in subset  $H$ , conditional to the simultaneous stimuli applied at all other nodes, the complementary set  $X - H$ . Formally,

$$I(H) = \mathcal{R}(H|X - H), \quad (6)$$

where  $\mathcal{R}$  is a generic response function. Note that the nodes in  $H$  are not stimulated, instead, they “passively listen” to the stimuli applied everywhere except on them. This definition could be applied for an arbitrary dynamical processes running on the network. In here, we consider the linear dynamical process above. Given the vector of unit stimuli  $\mathbf{s}(X - H)$  where  $s_i = 0$  if  $i \in H$  and  $s_i = 1$  for  $i \in X - H$ , the corresponding conditional temporal responses  $R(t, X - H)$  are

$$R(t; X - H) = (e^{Jt} - e^{J^0 t}) \mathbf{s}(X - H) \quad (7)$$

and the (temporally) accumulated pair-wise responses are

$$R_{ij}(X - H) = \int_0^\infty R_{ij}(t; X - H) dt. \quad (8)$$

Finally, the integration capacity of the selected nodes  $H$  is reduced to a number summing their responses:

$$I(H) = \sum_{i \in X-H; j \in H} R_{ij}(X - H). \quad (9)$$

For the results in Fig. 5b, the  $H$  is considered as the set of 30 ROIs with largest degree  $k$ , and  $X - H$  are the remaining 688 ROIs. The hub sets  $H$  are always ranked based on their global degree, as in Fig. 4a, but the selection for the different cases are based on the community the ROIs belong to, in either the anatomical or the network-based division. Hence, the colored bars all correspond to the integration capacity of 30 hubs, but only for those that belong to a specific module. The results in Fig. 5c are computed equivalently but considering hub sets  $H$  of increasing size, from  $|H| = 1$  to  $|H| = 170$ , adding one hub at a time to the set  $H$ .

**Segregation.** Here, we define segregation as the loss of communication suffered between the modules of a network, after a node or a set of nodes has been lesioned<sup>7</sup>. Let  $\mathcal{P}$  be a partition of a network into  $M$  modules, where  $C_m$  with  $m = 1, 2, \dots, M$  being the corresponding sets of nodes. We define modular integration  $I_{\mathcal{P}}(X)$  of the system  $X$ , as the amount of communication between modules. In this case, we evaluate  $I_{\mathcal{P}}(X)$  as the sum of pair-wise responses of the nodes in one module  $n$ , to the stimuli applied at the nodes of module  $m$ . Let  $R_{nm}$  be the reduced modular response matrix of size  $M \times M$ , evaluated summing the responses of all nodes in  $n$ , to stimuli applied at  $m$ ,

$$R_{nm}(X) = \sum_{i \in C_n; j \in C_m; n \neq m} R_{ij}. \quad (10)$$

Then, modular integration is calculated as the sum of the extradiagonal entries of matrix  $R_{nm}$ , such that:

$$I_{\mathcal{P}}(X) = \sum_{n,m=1; n \neq m}^M R_{nm}. \quad (11)$$

Assume now that a set of nodes  $H \subset X$  is lesioned, i.e., deleted from the network, and modular integration is re-computed for the same partition but in the lesioned network, namely,  $I_{\mathcal{P}}(X - H)$ . Segregation is thus defined as the (normalised) loss of modular integration in the network after the lesion of set  $H$ , compared to the modular integration in the original ‘healthy’ network:

$$S(H) = 1 - \frac{I_{\mathcal{P}}(X - H)}{I_{\mathcal{P}}(X)}. \quad (12)$$

For the segregation results in Fig. 5, first the reduced modular response matrix  $R_{nm}(X)$  and the corresponding modular integration  $I_{\mathcal{P}}(X)$  for the original-unlesioned-network were evaluated in both the anatomical and the network divisions. Then, targeted lesions were applied for various cases and the resulting modular integration  $I_{\mathcal{P}}(X - H)$  was recomputed. This implied to apply a lesion to the network for the chosen set of nodes  $H$  by deleting the corresponding rows and columns in the connectivity matrix  $A$ , and to recompute the resulting pair-wise response matrix for the lesioned connectivity, with stimulus vector  $\mathbf{s}(X - H)$  where  $s_i = 0$  if  $i \in H$  and  $s_i = 1$  for  $i \in X - H$ . Figure 5e reports the losses in modular integration between the modules,  $R_{nm}(X - H) / R_{nm}(X)$ , displayed as percentages, after the 30 nodes with largest degree had been lesioned. Figure 5f reports the segregation values when lesions were performed targeting either the 30 global hubs (black), or the 30 nodes with largest degree in each community (colored bars). Finally, the results were computed equivalently, but applying lesions of different sizes, from  $|H| = 1$  to  $|H| = 170$ , by orderly including the nodes with largest degree, one-by-one, to the lesioned set  $H$ .

## ACKNOWLEDGMENTS

We thank Egidio d’Angelo, Claudia Gandini Wheeler-Kingshott and Fulvia Palesi for the insightful and inspiring recommendations and discussions. This research was supported by (G.Z.L.) the European Union’s Horizon 2020 Framework Programme for Research and Innovation under the Specific Grant Agreement No. 945539 (Human Brain Project SGA3), (X.K.) a short-term fellowship of the European Molecular Biology Organization (Grant No. 7366), and (J.S.) is a FI fellow with the support of AGAUR, Generalitat de Catalunya and Fondo Social Europeo (2025 FI-2 00170).

## AUTHOR DECLARATION

Authors declare no conflicts of interest.

## REFERENCES

- <sup>1</sup>Joseph Parvizi. Corticocentric myopia: old bias in new cognitive sciences. *Trends Cogn. Sci.*, 13(8):354 – 359, 2009.
- <sup>2</sup>Luiz Pessoa. Understanding brain networks and brain organization. *Physics of Life Reviews*, 11:400–435, 2014.
- <sup>3</sup>J. A. Obeso, M. C. Rodríguez-Oroz, M. Stamelou, K. P. Bhatia, and D. J. Burn. The expanding universe of disorders of the basal ganglia. *The Lancet*, 384:521–531, 2014.
- <sup>4</sup>B. Attaallah, P. Petitot, R. Zambellas, S. Toniolo, M. R. Maio, A. Ganse-Dumrath S.R. Irani, S. G. Manohar, and M. Husain. The role of the human hippocampus in decision-making under uncertainty. *Nat. Hum. Behav.*, 8:1366–1382, 2024.
- <sup>5</sup>F. Palesi, J.-D. Tournier, F. Calamante, N. Muhler, G. Castellazzi, D. Chard, J. D. Tournier, G. Magenes, E. D’Angelo, and C. A. M. Wheeler-Kingshott. Contralateral cerebello-thalamo-cortical pathways with prominent involvement of associative areas in humans in vivo. *Brain Struct. Funct.*, 220:3369–3384, 2015.
- <sup>6</sup>F. Palesi, A. De Rinaldis, G. Castellazzi, F. Calamante, N. Muhler, D. Chard, J. D. Tournier, G. Magenes, E. D’Angelo, and C.A.M.G. Wheeler-Kingshott. Contralateral cortico-ponto-cerebellar pathways reconstruction in humans in vivo: implications for reciprocal cerebro-cerebellar structural connectivity in motor and non-motor areas. *Sci. Reps.*, 7:12841, 2017.
- <sup>7</sup>G. Zamora-López, C. S. Zhou, and J. Kurths. Cortical hubs form a module for multisensory integration on top of the hierarchy of cortical networks. *Front. Neuroinform.*, 4:1, 2010.
- <sup>8</sup>G. Zamora-López, C. S. Zhou, and J. Kurths. Exploring brain function from anatomical connectivity. *Front. Neurosci.*, 5:83, 2011.
- <sup>9</sup>Martijn P. van den Heuvel and Olaf Sporns. Rich-club organization of the human connectome. *J. Neurosci.*, 31(44):15775–15786, 2011.
- <sup>10</sup>M. Senden, G. Deco, M. A. de Reus, R. Goebel, and M. P. van den Heuvel. Rich club organization supports a diverse set of functional network configurations. *NeuroImage*, 96:174–178, 2014.
- <sup>11</sup>Mario Senden, Niels Reuter, Martijn P. van den Heuvel, Rainer Goebel, and Gustavo Deco. Cortical rich club regions can organize state-dependent functional network formation by engaging in oscillatory behavior. *NeuroImage*, 146:561 – 574, 2017.
- <sup>12</sup>M. A. Bertolero, B. T. T. Yeo, and M. D’Esposito. The modular and integrative functional architecture of the human brain. *Proc. Nat. Acad. Sci.*, 112(49):E6798–E6807, 2015.
- <sup>13</sup>N. A. Crossley, A. Mechelli, J. Scott, F. Carletti, P. T. Fox, P. McGuire, and E. T. Bullmore. The hubs of the human connectome are generally implicated in the anatomy of brain disorders. *Brain*, 137:2382–2395, 2014.
- <sup>14</sup>V. J. Kumar, K. Scheffler, and W. Grodd. The structural connectivity mapping of the intralaminar thalamic nuclei. *Sci. Reps.*, 13:11938, 2023.
- <sup>15</sup>P. T. Bell and J. M. Shine. Subcortical contributions to large-scale network communication. *Neurosci. Biobehav. Rev.*, 71:313–322, 2016.
- <sup>16</sup>J. Y. Hansen, S. Cauzzo, K. Singh, M. G. García-Gomar, J. M. Shine, M. Bianciardi, and B. Misic. Integrating brainstem and cortical functional architectures. *Nat. Neurosci.*, 2024.
- <sup>17</sup>D. C. van Essen, C. J. Donahue, and M. F. Glasser. Development and evolution of cerebral and cerebellar cortex. *Brain Behav. Evol.*, 91(3):158–169, 2018.
- <sup>18</sup>J. L. Ji, M. Spronk, K. Kulkarni, G. Repovš, A. Anticevic, and M. W. Cole. Mapping the human brain’s cortical-subcortical functional network organization. *NeuroImage*, 185:35–37, 2019.
- <sup>19</sup>J. W. Scannell and M. P. Young. The connective organization of neural systems in the cat cerebral cortex. *Curr. Biol.*, 3(4):191–200, 1993.
- <sup>20</sup>J. W. Scannell, C. Blakemore, and M. P. Young. Analysis of connectivity in the cat cerebral cortex. *J. Neurosci.*, 15(2):1463–1483, 1995.
- <sup>21</sup>C. C. Hilgetag, G. A. P. C. Burns, M. A. O’neill, J. W. Scannell, and M. P. Young. Anatomical connectivity defines the organization of clusters of cortical areas in the macaque monkey and the cat. *Phil. Trans. R. Soc. Lond. B*, 355:91–110, 2000.
- <sup>22</sup>C. C. Hilgetag and M. Kaiser. Clustered organisation of cortical connectivity. *Neuroinf.*, 2:353–360, 2004.
- <sup>23</sup>R. F. Betzel, J. D. Medaglia, L. Papadopoulos, G. L. Baum, R. C. Gur, R. E. Gur, D. Roalf, T. D. Satterthwaite, and D. S. Bassett. The modular organization of human anatomical brain networks: Accounting for the cost of wiring. *Network Neuroscience*, 1(1):42–68, 2017.
- <sup>24</sup>L. E. Suarez, Y. Yovel, Martijn P. van den Heuvel, O. Sporns, Y. Assaf, G. Lajoie, and B. Misić. A connectomics-based taxonomy of mammals. *Elife*, 11:e78635, 2022.
- <sup>25</sup>M. G. Puxeddu, J. Faskowitz, C. Seguin, Y. Yovel, Y. Assaf, R. F. Betzel, and O. Sporns. Relation of connectome topology to brain volume across 103 mammalian species. *PLoS Biol.*, 22(2):e3002489, 2024.
- <sup>26</sup>N. Ramnani. The primate cortico-cerebellar system: anatomy and function. *Nat. Rev. Neurosci.*, 7:511–522, 2006.
- <sup>27</sup>E. D’Angelo. Physiology of the cerebellum. In M. Manto and T.A.G.M. Huisman, editors, *The Cerebellum: From Embryology to Diagnostic Investigations*, volume 154 of *Handbook of clinical neurology*, chapter Physiology of the cerebellum, pages 85–108. Elsevier, Radarweg 29, PO Box 211, 1000 AE Amsterdam, Netherlands, 2018.
- <sup>28</sup>V. A. Traag, L. Waltman, and N. J. van Eck. From louvain to leiden: guaranteeing well-connected communities. *Sci. Reps.*, 9:5233, 2019.
- <sup>29</sup>M. Jacomy, T. Venturini, S. Heymann, and M. Bastian. Forceatlas2, a continuous graph layout algorithm for handy network visualization designed for the gephi software. *PLoS ONE*, 9(6):e98679, 2014.
- <sup>30</sup>R. Guimerà and L. A. N. Amaral. Cartography of complex networks: modules and universal roles. *J. Stat. Mech.*, P02001, 2005.
- <sup>31</sup>F. Klimm, J. Borge-Holthoefer, N. Wessel, J. Kurths, and G. Zamora-López. Individual node’s contribution to the mesoscale of complex networks. *New J. Phys.*, 16:125006, 2014.
- <sup>32</sup>G. Zamora-López, Y. Chen, G. Deco, M. L. Kringelbach, and C. S. Zhou. Functional complexity emerging from anatomical constraints in the brain: the significance of network modularity and rich-clubs. *Sci. Reps.*, 6:38424, 2016.
- <sup>33</sup>M. Gilson, N. E. Kouvaris, G. Deco, J.-F. Mangin, C. Poupon, S. Lefranc, D. Rivière, and G. Zamora-López. Network analysis of whole-brain fmri dynamics: A new framework based on dynamic communicability. *NeuroImage*, 201:116007, 2019.
- <sup>34</sup>G. Zamora-López and M. Gilson. An integrative dynamical perspective for graph theory and the analysis of complex networks. *Chaos: An Interdisciplinary Journal of Nonlinear Science*, 34:041501, 2024.
- <sup>35</sup>E. A. Phelps and J. E. LeDoux. Contributions of the amygdala to emotion processing: From animal models to human behavior. *Neuron*, 48:175–187, 2005.
- <sup>36</sup>J. J. Maller, T. Welton, M. Middione, F. M. Callaghan, J. V. Rosenfeld, and S. M. Grieve. Revealing the hippocampal connectome through super-resolution 1150-direction diffusion mri. *Sci. Reps.*, 9:2418, 2019.
- <sup>37</sup>C.-C. Huang, E. T. Rolls, C.-C. H. Hsu, J. Feng, and C.-P. Lin. Extensive cortical connectivity of the human hippocampal memory system: Beyond the “what” and “where” dual stream model. *Cereb. Cortex*, 21(10):4652–4669, 2021.
- <sup>38</sup>G. E. Alexander, M. R. DeLong, and P. L. Strick. Parallel organization of functionally segregated circuits linking basal ganglia

- and cortex. *Ann. Rev. Neurosci.*, 9:357–381, 1986.
- <sup>39</sup>S. N. Haber and R. Calzavara. The cortico-basal ganglia integrative network: The role of the thalamus. *Brain Res. Bull.*, 78:69–74, 2009.
  - <sup>40</sup>N. L. Benavidez, M. S. Bienkowski, M. Zhu, L. H. Garcia, M. Fayzullina, and et al. Organization of the inputs and outputs of the mouse superior colliculus. *Nat. Comms.*, 12:4004, 2021.
  - <sup>41</sup>Manuel A. Castro-alamancos and Barry W. Connors. Thalamo-cortical synapses. *Progress in neurobiology*, 51(6):581–606, 1997.
  - <sup>42</sup>Edward G Jones. The thalamic matrix and thalamocortical synchrony. *Trends Neurosci.*, 24(10):595–601, 2001.
  - <sup>43</sup>Stefan Knecht, Michael Deppe, Bianca Dräger, L Bobe, Hubertus Lohmann, E-B Ringelstein, and Henning Henningsen. Language lateralization in healthy right-handers. *Brain*, 123(1):74–81, 2000.
  - <sup>44</sup>Olumide A Olulade, Anna Seydell-Greenwald, Catherine E Chambers, Peter E Turkeltaub, Alexander W Dromerick, Madison M Berl, William D Gaillard, and Elissa L Newport. The neural basis of language development: Changes in lateralization over age. *Proc. Nat. Acad. Sci.*, 117(38):23477–23483, 2020.
  - <sup>45</sup>Paolo Bartolomeo and Tal Seidel Malkinson. Hemispheric lateralization of attention processes in the human brain. *Current opinion in psychology*, 29:90–96, 2019.
  - <sup>46</sup>Mutsutaka Kobayakawa. Left and right hemispheric contribution to social cognition. *Brain nerve*, 70(10):1067–1073, 2018.
  - <sup>47</sup>Mohua Das Gupta, Rahul Thakurta, and Anamitra Basu. Relationship between laterality and theory of mind among typical adults—a systematic literature review. *Acta Psychologica*, 254(104862), 2025.
  - <sup>48</sup>B.J. Baars. *A Cognitive Theory of Consciousness*. Cambridge University Press, 1988.
  - <sup>49</sup>A. R. Damasio. The brain binds entities and events by multiregional activation from convergence zones. *Neural Comp.*, 1:123–132, 1989.
  - <sup>50</sup>G. Tononi, O. Sporns, and G. M. Edelman. A measure for brain complexity: relating functional segregation and integration in the nervous system. *Proc. Nat. Acad. Sci.*, 91:5033–5037, 1994.
  - <sup>51</sup>M-Marsel Mesulam. From sensation to cognition. *Brain: a journal of neurology*, 121(6):1013–1052, 1998.
  - <sup>52</sup>Joaquin M Fuster. *Cortex and the mind: Unifying cognition*. Oxford University Press, 2005.
  - <sup>53</sup>J. G. White, E. Southgate, J. N. Thomson, and S. Brenner. The structure of the nervous system of the nematode *Caenorhabditis elegans*. *Phil. Trans. R. Soc. London B*, 314:1–340, 1986.
  - <sup>54</sup>Alex Arenas, Alberto Fernández, and Sergio Gómez. A complex network approach to the determination of functional groups in the neural system of *C. elegans*. In *Workshop on Bio-Inspired Design of Networks*, pages 9–18. Springer, 2007.
  - <sup>55</sup>L. A. Varshney, B. L. Chen, E. Paniagua, D. H. Hall, and D. B. Chklovskii. Structural properties of the *Caenorhabditis elegans* neuronal network. *PLoS Comput. Biol.*, 7(2):e1001066, 2011.
  - <sup>56</sup>O. Sporns, C. J. Honey, and R. Köster. Identification and classification of hubs in brain networks. *PLoS ONE*, 10:e1049, 2007.
  - <sup>57</sup>P. Hagmann, L. Cammoun, X. Gigandet, R. Meuli, C. J. Honey, V. J. Wedeen, and O. Sporns. Mapping the structural core of human cerebral cortex. *PLoS Biol.*, 6(7):e159, 2008.
  - <sup>58</sup>B. J. Baars. Global workspace theory of consciousness: toward a cognitive neuroscience of human experience. *Progress in Brain Research*, 150:45–53, 2005.
  - <sup>59</sup>M. Shanahan. *Embodiment and the inner life: Cognition and consciousness in the space of possible minds*, chapter Broadcast and the network. Oxford University Press, 2010.
  - <sup>60</sup>Morgan K Cambareri, Andreas Horn, Laura D Lewis, Jian Li, and Brian L Edlow. Subcortical hubs of brain networks sustaining human consciousness. *bioRxiv*, pages 2024–10, 2024.
  - <sup>61</sup>Jerome B Posner, Clifford B Saper, Nicholas D Schiff, and Fred Plum. *Plum and Posner’s diagnosis of stupor and coma*. Oxford University Press, 198 Madison Avenue, New York, New York 10016, 4th edition, 2007.
  - <sup>62</sup>David B Fischer, Aaron D Boes, Athena Demertzi, Henry C Evrard, Steven Laureys, Brian L Edlow, Hesheng Liu, Clifford B Saper, Alvaro Pascual-Leone, Michael D Fox, et al. A human brain network derived from coma-causing brainstem lesions. *Neurology*, 87(23):2427–2434, 2016.
  - <sup>63</sup>Evan S Lutkenhoff, Jeffrey Chiang, Luaba Tshibanda, Evelyn Kamau, Murielle Kirsch, John D Pickard, Steven Laureys, Adrian M Owen, and Martin M Monti. Thalamic and extrathalamic mechanisms of consciousness after severe brain injury. *Annals of neurology*, 78(1):68–76, 2015.
  - <sup>64</sup>Jitka Annen, Gianluca Frasso, Julia Sophia Crone, Lizette Heine, Carol Di Perri, Charlotte Martial, Helena Cassol, Athena Demertzi, Lionel Naccache, Steven Laureys, et al. Regional brain volumetry and brain function in severely brain-injured patients. *Annals of neurology*, 83(4):842–853, 2018.
  - <sup>65</sup>Pedro Nascimento Alves, Stephanie J Forkel, Maurizio Corbetta, and Michel Thiebaut de Schotten. The subcortical and neurochemical organization of the ventral and dorsal attention networks. *Communications Biology*, 5(1):1343, 2022.
  - <sup>66</sup>Camille Giacometti, Delphine Autran-Clavagnier, Audrey Dureux, Laura Viñales, Franck Lambertson, Emmanuel Procyk, Charles RE Wilson, Céline Amiez, and Fadila Hadj-Bouziane. Differential functional organization of amygdala-medial prefrontal cortex networks in macaque and human. *Comms. Biol.*, 7(1):269, 2024.
  - <sup>67</sup>Justine Beaujoin, Nicola Palomero-Gallagher, Fawzi Boumezeur, Markus Axer, Jeremy Bernard, Fabrice Poupon, Daniel Schmitz, Jean-François Mangin, and Cyril Poupon. Post-mortem inference of the human hippocampal connectivity and microstructure using ultra-high field diffusion mri at 11.7 t. *Brain Struct. and Funct.*, 223:2157–2179, 2018.
  - <sup>68</sup>François Lechanoine, Timothée Jacquesson, Justine Beaujoin, Barthélemy Serres, Mohammad Mohammadi, Alexia Planty-Bonjour, Frédéric Andersson, Fabrice Poupon, Cyril Poupon, and Christophe Destrieux. Wikibrainstem: an online atlas to manually segment the human brainstem at the mesoscopic scale from ultrahigh field mri. *NeuroImage*, 236:118080, 2021.
  - <sup>69</sup>FlyWire Consortium et al. Whole-brain annotation and multi-connectome cell typing of drosophila. *Nature*, 634(8032):139–152, 2024.
  - <sup>70</sup>Albert Lin, Runzhe Yang, Sven Dorkenwald, Arie Matsliah, Amy R Sterling, Philipp Schlegel, Szi-chieh Yu, Claire E McKellar, Marta Costa, Katharina Eichler, et al. Network statistics of the whole-brain connectome of drosophila. *Nature*, 634(8032):153–165, 2024.
  - <sup>71</sup>David C Van Essen, Stephen M Smith, Deanna M Barch, Timothy EJ Behrens, Essa Yacoub, Kamil Ugurbil, Wu-Minn HCP Consortium, et al. The wu-minn human connectome project: an overview. *NeuroImage*, 80:62–79, 2013.
  - <sup>72</sup>Kamil Ugurbil, Junqian Xu, Edward J Auerbach, Steen Moeller, An T Vu, Julio M Duarte-Carvajalino, Christophe Lenglet, Xiaoping Wu, Sebastian Schmitter, Pierre Francois Van de Moortele, et al. Pushing spatial and temporal resolution for functional and diffusion mri in the human connectome project. *NeuroImage*, 80:80–104, 2013.
  - <sup>73</sup>V. D. Blondel, J.-L. Guillaume, R. Lambiotte, and E. Lefebvre. Fast unfolding of communities in large networks. *J. Stat. Mech.*, 1008(10):6, 2008.
  - <sup>74</sup>Kawin Setsompop, R Kimmlingen, E Eberlein, Thomas Witzel, Julien Cohen-Adad, Jennifer A McNab, Boris Keil, M Dylan Tisdall, P Hoecht, Peter Dietz, et al. Pushing the limits of in vivo diffusion mri for the human connectome project. *NeuroImage*, 80:220–233, 2013.
  - <sup>75</sup>Andreas Horn, Martin Reich, Johannes Vorwerk, Ningfei Li, Gregor Wenzel, Qianqian Fang, Tanja Schmitz-Hübsch, Robert Nickl, Andreas Kupsch, Jens Volkmann, et al. Connectivity predicts deep brain stimulation outcome in parkinson disease. *Annals of neurology*, 82(1):67–78, 2017.
  - <sup>76</sup>Björn W Kreher, Irina Mader, and Valerij G Kiselev. Gibbs tracking: a novel approach for the reconstruction of neuronal

- pathways. *Magnetic Resonance in Medicine*, 60(4):953–963, 2008.
- <sup>77</sup>John Ashburner. A fast diffeomorphic image registration algorithm. *NeuroImage*, 38(1):95–113, 2007.
- <sup>78</sup>Andreas Horn and Felix Blankenburg. Toward a standardized structural–functional group connectome in mni space. *NeuroImage*, 124:310–322, 2016.
- <sup>79</sup>Matthew F Glasser, Timothy S Coalson, Emma C Robinson, Carl D Hacker, John Harwell, Essa Yacoub, Kamil Ugurbil, Jesper Andersson, Christian F Beckmann, Mark Jenkinson, et al. A multi-modal parcellation of human cerebral cortex. *Nature*, 536(7615):171–178, 2016.
- <sup>80</sup>James A Roberts, Alistair Perry, Gloria Roberts, Philip B Mitchell, and Michael Breakspear. Consistency-based thresholding of the human connectome. *NeuroImage*, 145:118–129, 2017.
- <sup>81</sup>Richard F Betzel, Alessandra Griffa, Patric Hagmann, and Bratislav Mišić. Distance-dependent consensus thresholds for generating group-representative structural brain networks. *Network Neuroscience*, 3(2):475–496, 2019.
- <sup>82</sup>Mária Ercsey-Ravasz, Nikola T Markov, Camille Lamy, David C Van Essen, Kenneth Knoblauch, Zoltán Toroczkai, and Henry Kennedy. A predictive network model of cerebral cortical connectivity based on a distance rule. *Neuron*, 80(1):184–197, 2013.
- <sup>83</sup>Szabolcs Horvát, Răzvan Gămănuț, Mária Ercsey-Ravasz, Loïc Magrou, Bianca Gămănuț, David C Van Essen, Andreas Burkhalter, Kenneth Knoblauch, Zoltán Toroczkai, and Henry Kennedy. Spatial embedding and wiring cost constrain the functional layout of the cortical network of rodents and primates. *PLoS Biol.*, 14(7):e1002512, 2016.
- <sup>84</sup>Ed Bullmore and Olaf Sporns. The economy of brain network organization. *Nat. Rev. Neurosci.*, 13(5):336–349, 2012.
- <sup>85</sup>S. Zhou and R.J. Mondragón. The rich-club phenomenon in the internet topology. *IEEE Comm. Lett.*, 8(3):180–182, 2004.
- <sup>86</sup>L. Katz and J. H. Powell. Probability distributions of random variables associated with a structure of the sample space of sociometric investigations. *Ann. Math. Stat.*, 28:442–448, 1957.
- <sup>87</sup>J. Reichardt and S. Bornholdt. Partitioning and modularity of graphs with arbitrary degree distribution. *Phys Rev. E*, 76:015102, 2007.
- <sup>88</sup>M. E. J. Newman and M. Girvan. Finding and evaluating community structure in networks. *Phys. Rev. E*, 69:026113, 2004.

Supplementary Information for:

## The global communication pathways of the human brain transcend the cortical - subcortical - cerebellar division

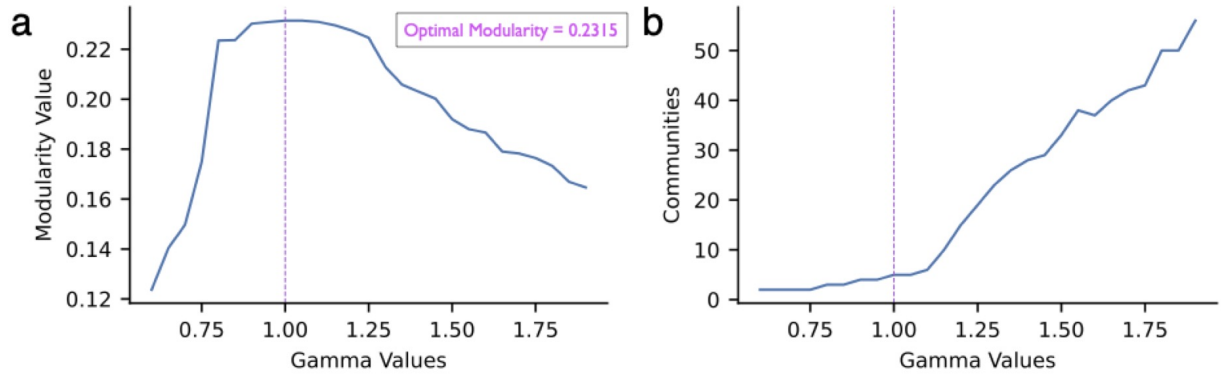


FIG. S1. **Community Detection, finding optimal modularity over different gamma values.** **a**, Optimal modularity value (over 100 iterations per gamma value) for different resolution parameters gamma. **b** The number of communities of the optimal partitioning for different resolution parameters.

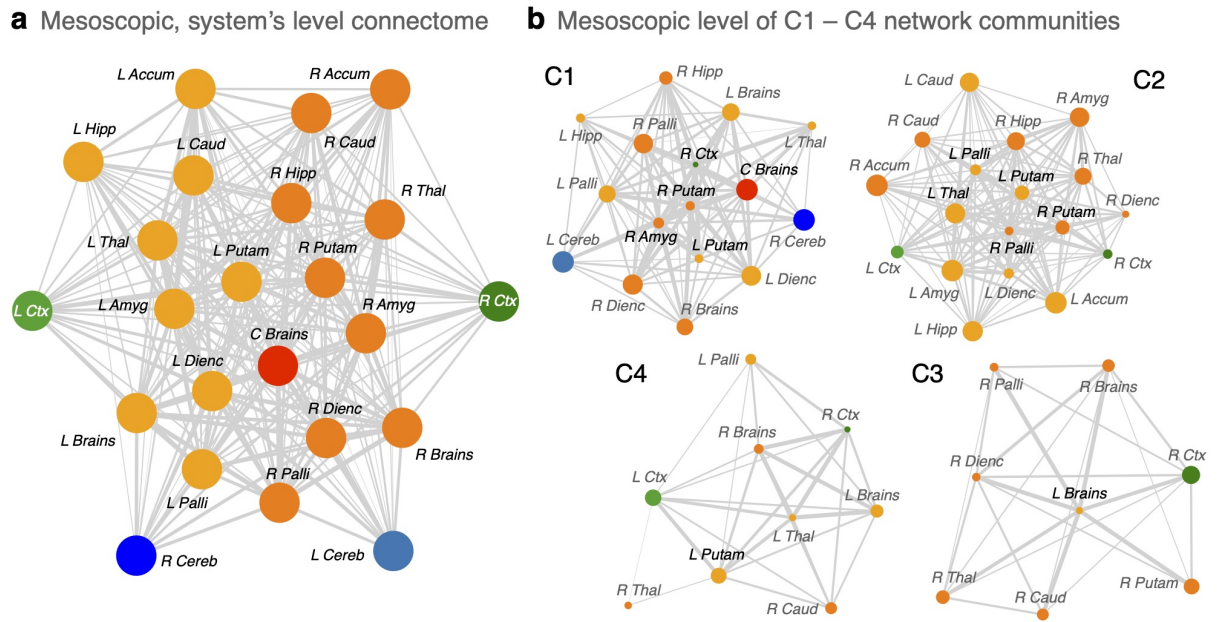


FIG. S2. Visualization of the structural connectivity at the level of anatomical components comprising the cortex, the cerebellum and nine subcortical nuclei; **a** for the brain-wide network and **b** the subnetworks representing network communities C1 to C4. Community C5 is omitted for its simplicity as it only contains three regions. Node diameters are proportional to the fraction of ROIs that each anatomical component dedicates to the community. Hence, all diameters are equal in **a**. Link widths reflect the connection probability between components, measured as the fraction of ROIs in both components that are connected, relative to all possible connections they could have (if all ROIs in both components were connected).